Probing the Function of Conserved Residues in the Serine/Threonine Phosphatase PP2Cα†

Michael D. Jackson, Clark C. Fjeld, and John M. Denu*

Oregon Health & Science University, Department of Biochemistry and Molecular Biology, Portland, Oregon 97201-3098

Received January 15, 2003; Revised Manuscript Received April 30, 2003

ABSTRACT: Human PP2Cα is a metal-dependent phosphoserine/phosphothreonine protein phosphatase and is the representative member of the large PPM family. The X-ray structure of human PP2Cα has revealed an active site containing a dinuclear metal ion center that is coordinated by several invariant carboxylate residues. However, direct evidence for the catalytic function of these and other active-site residues has not been established. Using site-directed mutagenesis and enzyme kinetic analyses, we probed the roles of conserved active-site amino acids within PP2Cα. Asp-60 bridges metals M1 and M2, and Asp-239 coordinates metal M2, both of which were replaced individually to asparagine residues. These point mutations resulted in ≥1000-fold decrease in k_{cat} and ≥30-fold increase in K_m value for Mn^{2+}. Mutation of Asp-282 to asparagine caused a 100-fold decrease in k_{cat}, but no significant effect on K_m values for metal and substrate, consistent with Asp-282 activating a metal-bound water nucleophile. Mutants T128A, E37Q, D38N, and H40A displayed little or no alterations on k_{cat} and K_m values for substrate or metal ion (Mn^{2+}). Analysis of H62Q and R33A yielded k_{cat} values that were 20- and 2-fold lower than wild-type, respectively. The mutant R33A showed a 8-fold higher K_m for substrate, while the K_m observed with H62Q was unaffected. A pH−rate profile of the H62Q mutant showed loss of the ionization that must be protonated for activity. Brönsted analysis of substrate leaving group pK_a values for H62Q indicated a greater dependency (slope −0.84) on leaving group pK_a in comparison to wild-type (slope −0.33). These data provide strong evidence that His-62 acts as a general acid during the cleavage of the P−O bond.

Phospho-protein phosphatases are generally grouped into the protein tyrosine phosphatases (PTPs) and the phosphoserine/phosphothreonine-specific phosphatases (PPs), based on substrate specificity and genetic homology (*1*−*3*). The PPs can be divided into two large gene families, designated PPP and PPM. While both families are metal-dependent phosphatases, the PPM family has long been distinguished by its dependence upon the divalent metal atoms of manganese or magnesium as well as their resistance to several inhibitors that are effective toward the PPP family of phosphatases (*2*, *4*−*7*). Human PP2Cα is the defining member of the PPM family and is evolutionarily conserved from prokaryotes to eukaryotes and appears to have a prominent role in negatively regulating stress responses within the cell. Mammalian PP2C exists as two major isoforms, PP2Cα and PP2C*β*. PP2Cα has been shown to dephosphorylate and inactivate the mitogen-activated protein kinase (MAPK) p38 (*8*) as well as regulate the *c*-Jun N-terminal kinase pathway (*9*). The PP2C phosphatase family has been implicated in other signal transduction pathways as well. Recent work by Strovel et al. have shown that PP2C*β*-1 is a positive regulator of LEF-1-dependent transcription by dephosphorylating Axin (*10*), which is a negative regulator of the *Wnt* signaling pathway. Leung-Hagesteijn et al. have identified a PP2C family member (ILKAP), which deactivates integrin-linked kinase, ILK1, a kinase that is also involved in the regulation of the *Wnt* signaling pathway (*11*). Reports have also suggested a PP2C-like phosphatase as a negative regulator of cystic fibrosis transmembrane conductance regulator (CFTR) in airway and intestinal epithelia (*12*), and has been shown to be associated with CFTR based on co-immunoprecipitation and cross-linking experiments (*13*). These observations place the PP2C family of protein phosphatases in important roles within numerous signal transduction pathways and intracellular processes.

The crystal structure of human PP2Cα bound with Mn^{2+} and phosphate has implicated several residues in metal binding (*14*). The active site of PP2Cα contains invariant carboxylate-containing residues that coordinate two metals, M1 and M2, which are 4 Å apart (Figure 1). The two metal centers share the carboxylate side chain of Asp-60 and a water molecule, which has been proposed as the nucleophilic water molecule utilized in the dephosphorylation of substrate (*14*). Metal M1 is coordinated by four water molecules and makes only two direct contacts with the active site, the backbone carbonyl of Gly-61 and the carboxylate residue of Asp-60. Glu-37 and Asp-38 interact indirectly with M1 via hydrogen bonds with metal-bound water molecules (Figure 1). Metal M2 is coordinated to three water molecules, the bridging carboxylate of Asp-60, as well as Asp-239 and Asp-282. An arginine residue (Arg-33) was shown to hydrogen bond to inorganic phosphate in the crystal structure.

† This work was supported by NIH Grant GM59785 to J.M.D. and NIH postdoctoral fellowship DK07680−12 to M.D.J.

* Corresponding author. Oregon Health & Science University, Department of Biochemistry and Molecular Biology, 3181 SW Sam Jackson Park Road, Portland, OR 97201-3098. Phone: (503) 494-0644. Fax: (503) 494-8393. E-mail: denuj@ohsu.edu.

10.1021/bi034074+ CCC: $25.00
Published on Web 06/26/2003

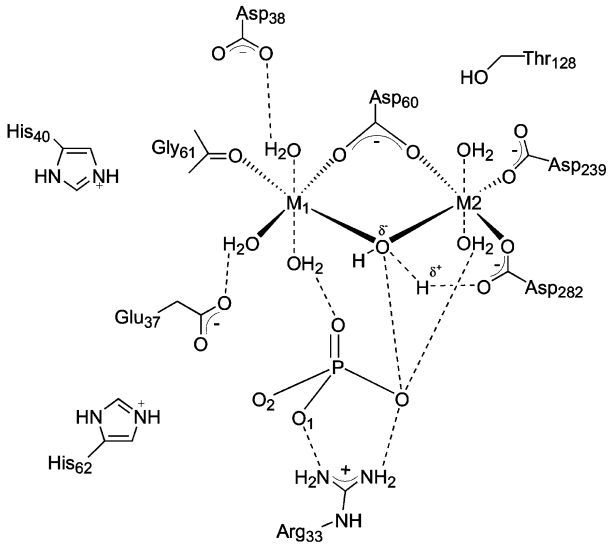

FIGURE 1: Schematic representation of the ligand environment in human PP2Cα based on the X-ray crystal structure reported by Das et al. (*14*). The bound phosphate coordinates to the metal centers M1 and M2 through hydrogen-bonding interactions with water ligands, as well as electrostatic interaction with Arg-33. Asp-60 bridges the two metal ions, while Asp-239, Asp-282, and Gly-61 (backbone carbonyl) make direct contact with the metal centers. Glu-37 and Asp-38 hydrogen bond to two water molecules that serve as direct ligands to M1. Although conserved residues His-40 and His-62 do not make contact with this coordination shell, they are within the active site pocket. Thr-128 is hydrogen bonded to Asp-60 through the main chain N−H.

With the exception of the bridging water molecule, no other nucleophile was identified or proposed (*14*). Within several angstroms of the metal center, two conserved histidine residues (His-40 and His-62) and a threonine (Thr-128) residue exist. The functions of these residues has not been suggested nor tested. Because the crystal structure of PP2Cα was obtained at pH 5.0, where the enzyme is incorrectly protonated and only ∼0.1% active, the actual roles of many of the conserved residues are in question. To investigate the role of residues Arg-33, Glu-37, Asp-38, His-40, Asp-60, His-62, Thr-128, Asp-239, and Asp-282 in catalysis and metal/substrate binding, these residues have been mutated and the resulting mutants analyzed using steady-state and rapid reaction kinetics, pH studies, and Brönsted analysis.

MATERIALS AND METHODS

Reagents. 6,8-Difluoro-4-methylumbelliferyl phosphate (DiFMUP), 8-fluoro-4-methylumbelliferyl phosphate (8FMUP), and 4-methylumbelliferyl phosphate were obtained from Molecular Probes (Eugene, OR). All chemicals were of the highest purity commercially available and were purchased from Sigma (St. Louis, MO), Aldrich (Milwaukee, WI), or Fisher Scientific (Pittsburgh, PA), and were used without further purification.

Site-Directed Mutagenesis. Site-directed mutagenesis of residues Arg-33, Glu-37, Asp-38, His-40, Asp-60, His-62, Thr-128, Asp-239, and Asp-282 were carried out as described previously using the BioRad Muta-gene method (*15*). All mutations were verified by DNA sequencing.

Overexpression and Purification of Wild-Type and Mutant PP2Cα Proteins. The overexpression and purification of PP2Cα have been previously described (*16*). The overexpression and purification of PP2Cα mutants utilized the same protocols as that used for wild-type PP2Cα and were performed without modification.

General Assay Conditions. All enzyme assays were performed in a three-component system containing 0.1 M acetate, 0.05 M Tris (Tris-(hydroxymethyl)amino-methane), and 0.05 M Bis-Tris (Bis[2-Hydroxyethyl]imino-tris[hydroxymethyl]methane) (TBA) at 25 °C, 1 mM DTT, and 0.1−15 μM enzyme. The TBA buffer system maintains a constant ionic strength of 0.1 M throughout the entire pH range. To determine the kinetic parameters k_{cat} and k_{cat}/K_m for *p*NPP, the initial velocities were measured at *p*NPP concentrations ranging from 1 to 200 mM (dependent upon enzyme activity) at saturating levels of Mn^{2+} (20−200 mM, dependent upon enzyme used), and the data were fitted to eq 1 using the computer program KaleidaGraph (Abelbeck Software). To determine the kinetic parameters of k_{cat} and k_{cat}/K_m for metal, Mn^{2+} concentrations ranging from 1 to 200 mM were used (dependent on enzyme) under saturating concentrations of *p*NPP (10−200 mM). Two types of assays were used to monitor PP2Cα phosphatase activity and are described below. Saturating amounts of divalent metal atom, Mn^{2+} (20−200 mM, depending on enzyme) was used in all steady-state and pre-steady-state experiments with the exception of pH dependence and phosphate inhibition studies, in which case saturating amounts of Mg^{2+} (40 mM) was used. Initial velocities were determined from the linear portion of the kinetic traces to ensure true steady state conditions for all assays used.

$$v = (k_{cat}[E]_t[S])/(K_m + [S]) \quad (1)$$

Continuous Assay. The continuous assay monitoring the dephosphorylation of the artificial substrate, *p*-nitrophenyl phosphate (*p*NPP), was performed using a Labsystems Multiscan Acsents photometric microplate reader (Franklin, MA) by monitoring the absorbance change recorded at 405 nm, pH 8.0 over the course of 5−30 min, depending on the enzyme used. Initial linear rates were determined using the molar extinction coefficient (ε) of 16.3 or 8.9 mM^{-1} cm^{-1} for the product *p*-nitrophenol (*p*NP) at 405 nm in pH 8.0 or pH 7.0 buffer, respectively.

Endpoint Assay. Two end point assays were used to measure PP2Cα activity. In all cases, assay conditions were identical to those described under "General Assay Conditions". Reactions were incubated at 25 °C for 5−30 min, depending on enzyme used, and then quenched using the phosphate detection assay. The phosphate detection assay was used for measuring the initial rates of dephosphorylation of amino acids and aryl substrates. The release of phosphate was determined using the colorimetric method described by Brotherus et al. with slight modifications (*17*). Briefly, 300 μL enzyme assays were terminated with the addition of 0.5 mL of 0.5 N HCl containing 15 mg of ascorbic acid, 2.5 mg of ammonium heptamolybdate, and 5 mg of sodium dodecyl sulfate. The resulting mixture was incubated at 4 °C for 10 min. For color development, 750 μL of developer containing 15 mg of sodium arsenite, 15 mg of ascorbic acid, and 15 μL of glacial acetic acid were added and the resulting solution was incubated at 35 °C for 5 min. The samples were removed from the water bath and incubated for an additional 20 min at room temperature. The absorbance was then read

at 850 nm using a Shimadzu BioSpec-1601 UV−visible spectrophotometer. The concentration of free phosphate was determined using a standard curve generated from phosphate standards of known concentrations. The second endpoint assay using 0.5 M EDTA, pH 10.0 has been described (*16*) and was used without modification.

Steady-State Kinetic Analyses. The end point assay using the EDTA stop solution was used to measure the pH dependence of wild-type PP2Cα activity as well as H40A and H62Q activity for the generation of pH profiles. The values of k_{cat} and k_{cat}/K_{pNPP} were obtained at pH values ranging from 5.5 to 10.6 with *p*NPP as the varied substrate (0.1−20 mM for wild-type and H62Q, 1−200 mM for R33A) at saturating levels of Mn^{2+} (10 mM) or Mg^{2+} (40 mM). The pH data for Mn^{2+} and Mg^{2+} were fitted to eqs 2 and 3, respectively, where *C* is the pH-independent value of either k_{cat} or k_{cat}/K_{pNPP}, H is the proton concentration, and K_a and K_b are the ionization constants of the groups involved in the reaction.

$$v = C/(1 + H/K_a) \quad (2)$$

$$v = C/(1 + H/K_a + K_b/H) \quad (3)$$

The extent of wild-type PP2Cα, R33A, and H62Q inhibition by inorganic phosphate (P_i) was determined using the continuous assay described above. Assays included Mg^{2+} instead of Mn^{2+} to prevent precipitation of the metal. Continuous assays were generated by varying *p*NPP concentrations (0.1−20 mM for wild-type and H62Q, 1−200 mM for R33A) in the presence of saturating amounts of Mg^{2+} (40 mM) at fixed concentrations of the product, P_i at concentrations ranging from 0.1 to 10 mM. At higher P_i concentrations, a white precipitate formed during the reaction. Sodium chloride was added to the reactions and controls to maintain a constant ionic strength. The inhibition of P_i on the catalytic activity of wild-type and mutants was competitive with respect to *p*NPP, and the data were fitted to eq 4, where *I* is the inhibitor concentration, E_t is the total enzyme concentration, *S* is the *p*NPP concentration, and K_{is} is the inhibition constant.

$$v = (k_{cat}[E]_t[S])/([S] + K_m(1 + [I]/K_{is})) \quad (4)$$

The leaving group dependence of PP2Cα was analyzed by determining the dephosphorylation rate (k_{cat}) of several artificial compounds, which differ by the pK_a of the leaving group. Substrates 6,8-difluoro-4-methylumbelliferyl phosphate (DiFMUP) (pK_a = 4.6), 8-fluoro-4-methylumbelliferyl phosphate (pK_a = 6.4), *p*NPP (pK_a = 7.1), 4-methylumbelliferyl phosphate (pK_a = 7.8), β-naphthyl phosphate (pK_a = 9.38), phenyl phosphate (pK_a = 9.99), and phosphoserine (pK_a = 14.1) were analyzed in TBA buffer (pH 7.0) as described above. Dimethylsulfoxide (DMSO) was added to some substrates to increase solubility when analyzing the R33A mutant. Control reactions using R33A and varying concentrations of *p*NPP in the presence of up to 10% DMSO showed no effect on the rate of the reaction or substrate K_m. Enzyme concentrations ranged from 0.1 to 15 mM, and was dependent upon the enzyme used. For the generation of saturation curves, substrate concentrations ranging from 0.1 to 10 mM for wild-type and H62Q mutant and 1 to 200 mM for R33A were used, depending on substrate K_m. Enzyme activity was monitored using the phosphate detection assay at pH 7.0. Brönsted values were obtained by linear least-squares fitting of log(k_{cat}) versus pK_a of the leaving group for the substrates using the computer program KaleidaGraph (Abelbeck Software).

Pre-Steady-State Kinetics. Enzyme (concentrations of PP2Cα, R33A, and H62QA were 10, 20, and 40 μM, respectively) and substrate (40 mM for wild-type and H62Q; 300 mM for R33A) were rapidly mixed at pH 8.0 and 25 °C in a temperature-controlled SF-61 stopped-flow spectrophotometer (Hi-Tech Scientific). The absorbance of *p*NP was monitored at 410 nm for a total reaction time of 1.75 s. The wild-type or mutant enzymes were combined with Mn^{2+} (20 mM) in reaction buffer (TBA, pH 8.0) prior to rapid mixing with substrate also in the same reaction buffer. The final concentration of Mn^{2+} was 10 mM, and *p*NPP concentrations were held at 20 mM for wild-type and H62Q enzymes, and 150 mM for the R33A mutant. The data obtained from wild-type PP2Cα and R33A were fitted to eq 5 using the computer program KaleidaGraph (Abelbeck Software), where *A* is the amplitude of the burst, *k* is the first-order rate of the burst, *B* is the slope of the linear portion of the curve, *C* is the intercept of the line, and *t* is time. For H62Q, the data was fitted using linear least-squares.

$$\text{absorbance} = Ae^{-kt} + Bt + C \quad (5)$$

RESULTS AND DISCUSSION

Probing the Functions of the Proposed Metal−Ligand Residues. Steady-State Kinetic Analysis. A detailed kinetic analysis of wild-type PP2Cα has been reported previously (*16*). Though both Mn^{2+} and Mg^{2+} can activate PP2Cα, the Mn^{2+} bound form of the enzyme yields a k_{cat} value that is 25-fold faster, and a K_m for metal ion that is 15-fold lower, compared with the Mg^{2+} activated form (*16*). Using the commonly employed artificial substrate *p*NPP, a pH−rate analysis identified two critical ionizations having pK_a values of ∼7.5 and ∼9 for a group that must be unprotonated and one that must be protonated for activity (k_{cat}/K_m), respectively. At pH 7 using *p*NPP as substrate, the rate-limiting step is cleavage of the P−O bond, whereas, at pH 8.5, phosphate release limits turnover (*16*). The group with a pK_a of ∼7.5 is thought to represent the metal-bound water molecule, which acts as the nucleophile during the direct attack at the phosphorus center of substrate. The group with a pK_a of ∼9 may represent the general acid, which protonates the leaving group oxygen during P−O bond scission.

Here, we investigate the functions of conserved active-site residues using site-directed mutagenesis and a variety of kinetic analyses. For the purpose of clarity, active site residues were grouped into those that contact the two metal ligands directly or indirectly through a water molecule (Asp-60, Asp-239, Asp-282, Glu-37, and Asp-38), and those that do not (Arg-33, His-40, His-62, and Thr-128) (Figure 1).

To determine the role of the residues that directly bind to the metal centers, Asp-60, Asp-239, and Asp-282 were mutated individually to asparagine. The corresponding mutants were analyzed using steady-state kinetics to evaluate the effect of the mutation on substrate or metal binding, as well as catalysis. To determine the kinetic parameters k_{cat} and k_{cat}/K_m for both substrate and metal, the initial velocities

Table 1: Steady-State Kinetic Parameters for Wild-Type PP2Cα and Mutants E37Q, D38N, D60N, D239N, and D282N[a]

enzyme	k_{cat} s^{-1}	K_{pNPP} mM	K_{metal} mM	k_{cat}/K_{pNPP} M^{-1} s^{-1}	k_{cat}/K_{metal} M^{-1} s^{-1}
wild-type PP2Cα	5.16 ± 0.26	4.67 ± 0.31	1.04 ± 0.02	1100 ± 90	4960 ± 100
E37Q	2.98 ± 0.03	3.62 ± 0.14	1.06 ± 0.03	827 ± 23	2800 ± 46
D38N	8.66 ± 0.69	6.83 ± 0.17	1.46 ± 0.03	1340 ± 40	5580 ± 82
D60N	0.006 ± 0.0002	2.58 ± 0.1	43.9 ± 0.6	2.26 ± 0.03	0.138 ± 0.003
D239N	0.0013 ± 0.00003	1.07 ± 0.03	28.6 ± 1.1	1.22 ± 0.03	0.044 ± 0.001
D282N	0.052 ± 0.015	6.32 ± 0.12	1.16 ± 0.05	9.79 ± 0.07	35.1 ± 0.6

[a] All assays were performed in Tris/Bis-Tris/acetate buffer at pH 8.0 and 25 °C with saturating levels of either *p*NPP (20 mM) or Mn^{2+} (15−100 mM). Reactions were monitored at 405 nm as outlined in Materials and Methods. All data were fitted to the Michaelis−Menten equation using nonlinear least squares regression (Kaleidagraph graphing software). The data displayed are the average (with standard deviation) from at least three independent experiments.

Table 2: Steady-State Kinetic Parameters for Wild-Type PP2Cα and Mutants R33A, H40A, H62Q, and T128A[a]

enzyme	k_{cat} s^{-1}	K_{pNPP} mM	K_{metal} mM	k_{cat}/K_{pNPP} M^{-1} s^{-1}	k_{cat}/K_{metal} M^{-1} s^{-1}
wild-type PP2Cα	5.16 ± 0.26	4.67 ± 0.31	1.04 ± 0.02	1100 ± 90	4960 ± 100
R33A	2.05 ± 0.02	35.9 ± 0.6	1.17 ± 0.02	52.1 ± 0.3	1080 ± 32
H40A	5.14 ± 0.09	4.61 ± 0.1	1.09 ± 0.03	1110 ± 30	4720 ± 170
H62Q	0.25 ± 0.004	6.90 ± 0.28	0.59 ± 0.02	36 ± 0.2	420 ± 3
T128A	5.56 ± 1.11	3.96 ± 0.16	2.78 ± 0.5	1400 ± 38	2000 ± 51

[a] All assays were performed in Tris/Bis-Tris/acetate buffer at pH 8.0 and 25 °C with saturating levels of either *p*NPP (20−200 mM) or Mn^{2+} (15 mM). Reactions were monitored at 405 nm as outlined in Materials and Methods. All data were fitted to the Michaelis−Menten equation using nonlinear least squares regression (Kaleidagraph graphing software). The data displayed are the average (with standard deviation) from at least three independent experiments.

were measured at various substrate or metal concentrations, and the data were fitted to the Michaelis−Menten equation, as detailed in Materials and Methods. The results are summarized in Table 1. Mutation of these residues caused a dramatic reduction in activity. In terms of k_{cat} values, the D239N, D60N, and D282N mutants were 4000-, 900-, and 100-fold lower than that for wild-type enzyme, respectively. Interestingly, the K_m for *p*NPP displayed little change, though the K_m for Mn^{2+} was increased greatly for D60N and D239N, but not for D282N. In fact, the D282N mutant displayed the same ~100 fold effect on both k_{cat}/K_m and k_{cat} values, without any significant change in either K_m value. These observations suggest that Asp-282 may have a more important role in catalysis than in binding either substrate or metal. Careful analysis of the crystal structure revealed that Asp-282 not only coordinates M2, but also is hydrogen bonded (2.71 Å) to the metal-bridged water molecule that is poised for attack on the phosphorus atom (Figure 1). Das et al. did not note this observation (*14*). Asp-282 is the only residue in the active site of PP2Cα that makes direct contact to the proposed water nucleophile (*14*). Changing Asp-282 to Asn does not appear to alter metal binding, suggesting that M2 coordination at this position does not require a formal negative charge. However, to function during catalysis, an aspartate is critical at this position. Asp-282 may position the water molecule for in-line attack on the phosphate, or more likely, may function to assist in deprotonating the water nucleophile. The data obtained with D60N and D239N are consistent with these residues functioning in metal binding and catalysis as first proposed by Das et al (*14*).

To determine the role of the residues that indirectly bind to the metal centers, Glu-37 and Asp-38 were mutated to glutamine and asparagine, respectively, and analyzed as described above. Glu-37 and Asp-38 hydrogen bond to two different water molecules that are ligands to metal M1 (Figure 1). Surprisingly, very little effect on k_{cat}, K_m (for *p*NPP and metal), and k_{cat}/K_m values were observed (less than 2-fold in either direction) for E37Q and D38N enzymes (Table 1). This observation is in sharp contrast to the results with D60N, D239N, and D282N, where even the most conservative substitution caused dramatic effects on catalysis. The lack of significant effects with the E37Q and D38N mutants suggests that these conservative substitutions do not compromise their hydrogen bonding interaction with the inner shell water molecules coordinated to metal M1.

Analysis of Conserved Residues Not Proposed in Metal Binding. Steady-State Kinetic Analysis of R33A, H40A, H62Q, and T128A. The functions of Arg-33, His-40, His-62, and Thr-128 were probed by creating the mutant PP2Cα enzymes R33A, H40A, H62Q, and T128A, respectively. The steady-state kinetic parameters k_{cat}, K_m for both metal and substrate (*p*NPP), and k_{cat}/K_m for both metal and substrate were obtained for wild-type PP2Cα and the mutant enzymes, H40A, H62Q, R33A, and T128A (Table 2). At pH 8.0, the kinetic data obtained for the H40A mutant was indistinguishable from that obtained for wild-type PP2Cα (Table 2). Also of interest was the mutation of Thr-128, which in the reported crystal structure is hydrogen-bonded to Asp-60 through the main chain NH (*14*). Asp-60 is coordinated to both metal ions and bridges them at a distance of 4 Å. Analysis of T128A showed little effect upon k_{cat} or K_m for substrate, with minor effects on the K_m for Mn^{2+} and k_{cat}/K_{metal}. These data suggest that the hydrogen bonding interaction observed in the structure between Asp-60 and Thr-128 is not necessary for catalysis and metal/substrate binding.

The R33A mutant lacks the arginine residue proposed to participate in substrate binding and catalysis. This mutant exhibited slight changes in k_{cat}, K_m, and k_{cat}/K_m (Table 2) for metal, but the K_m value for substrate had decreased by almost 8-fold. The H62Q mutant showed only slight changes (<2-fold) in K_m for *p*NPP and for metal ion compared with wild-type enzyme. However, the H62Q mutant was 20−30-fold less active (comparing k_{cat}/K_m for *p*NPP and k_{cat} values) than native PP2Cα, indicating that substitution at residue 62 (histidine for glutamine) greatly affects catalysis. The lack of any significant changes to K_m values suggests that His-

62 contributes little to substrate and metal binding. When His-62 was replaced with Ala, the resulting mutant displayed no detectable activity (data not shown), suggesting that glutamine at this position may partially fulfill function by maintaining the proper bulk in the cavity, or by maintaining important hydrogen bonding interactions within the active site.

Phosphate Inhibition Studies. To provide additional support that Arg-33 functions in substrate binding (via the phosphate group), phosphate inhibition studies were performed with R33A, and with wild-type PP2Cα and H62Q for comparison. The resulting value of K_i is the true dissociation constant for phosphate binding, and provides a more direct measure of changes in binding affinity compared with the K_m values for substrate. Because the H62Q mutant shows a minimal effect on K_{pNPP}, it was predicted that the K_i for phosphate would be very similar to that of wild-type enzyme. For each series of assays, the concentration of *p*NPP was varied in the presence of various fixed concentrations of free phosphate and at saturating levels of Mg^{2+}. Double reciprocal plots of wild-type PP2Cα and H62Q revealed a series of lines that intersected on the *y*-axis, representing competitive inhibition (Figure 2). The inhibition constant K_{is} for wild-type PP2Cα and H62Q was 0.78 ± 0.02 and 1.27 ± 0.02 mM, respectively. A double reciprocal plot of R33A was also generated, but phosphate concentrations higher than 10 mM could not be used due to the formation of a precipitate at higher concentrations (data not presented). The K_{is} for R33A from this analysis was 9.7 ± 0.6 mM, or ~10-fold higher than that of wild-type enzyme or the H62Q mutant. These data are consistent with Arg-33 contributing a small but significant role in phosphate binding. In PP2Cα, direct hydrogen-bonding interactions of the phosphate with two metal-bound water molecules (*14*) may contribute a significant portion of the substrate binding energy. Moreover, in more distantly related PP2C genes, Arg-33 (PP2Cα numbering) is not invariant (*14*).

Determining the Rate-Limiting Step for H62Q and R33A Using Pre-Steady-State Kinetics. To determine whether the chemistry step was affected in the H62Q catalyzed reaction, pre-steady-state kinetic analyses were performed with H62Q. For comparison, the R33A mutant was also analyze. Initial analysis of PP2Cα using pre-steady-state kinetics yielded a rapid formation ("burst") of *p*NP product followed by a slower steady-state phase at pH 8.5 (*16*). The presence of an initial "burst" of product indicates that an event after chemistry is rate-limiting in turnover. The burst rate is a measure of the rate of P−O bond cleavage. Thus, pre-steady-state kinetics can be diagnostic for changes in rate-limiting steps. If the mutations at positions Arg-33 and His-62 affect chemical catalysis, these mutations would make chemistry more rate limiting, if additional steps were unaffected. A decrease in the burst rate or a loss of the burst phase would suggest that the chemistry step is slow relative to other subsequent steps. Using a stopped-flow spectrophotometer, the rapid reaction of R33A or H62Q with *p*NPP was followed by measuring the formation of *p*NP. Compared with wild-type enzyme (Figure 3), R33A displayed a rapid product burst phase followed by a slower linear rate. As with wild-type enzyme (*16*), the amplitude of the burst correlated with the initial concentration of R33A. The burst phase yielded an apparent first-order rate constant of 3.31 ± 0.03 s^{-1}, which

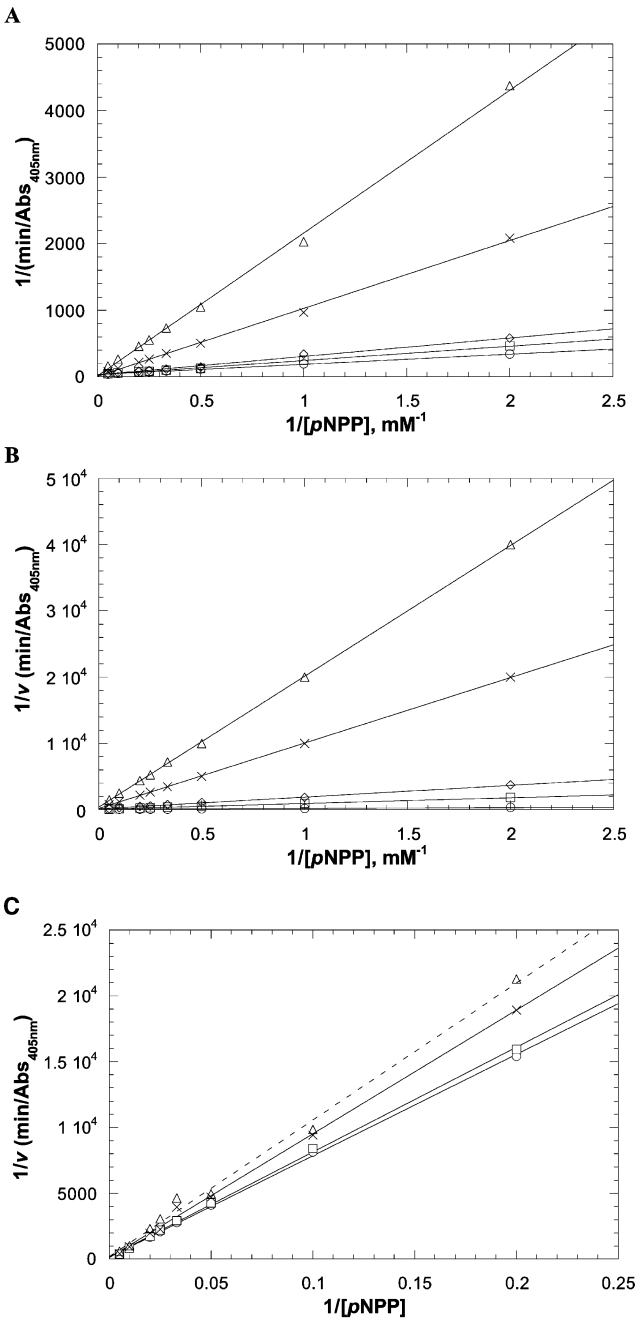

FIGURE 2: Phosphate inhibition of wild-type PP2Cα H62Q and R33A. (A) Double reciprocal plot ($1/v$ vs $1/[p\text{NPP}]$) at varied fixed [phosphate] using wild-type PP2Cα; (B) H62Q; and (C) R33A. The assays were performed at saturating Mg^{2+} concentrations (40 mM). All plots represent competitive inhibition with respect to *p*NPP. The K_{is} of 0.78 ± 0.02, 1.27 ± 0.02, and 9.7 ± 0.6 mM were determined for wild-type, H62Q and R33A, respectively, as described under Materials and Methods. The phosphate concentrations were as follows: open circles, 0 mM sodium phosphate; open squares, 0.5 mM sodium phosphate; open diamonds, 1 mM sodium phosphate; the symbol "x", 5 mM sodium phosphate; open triangles, 10 mM sodium phosphate. All assays were performed as outlined under Materials and Methods.

is ~6-fold slower than that observed with wild-type enzyme at pH 8.5 (*16*). This slight change in burst rate is in reasonable agreement with the 2.5-fold lower k_{cat} observed with R33A mutant compared with wild-type enzyme at pH 8. Together these data suggest that Arg-33 does not play a considerable role during P−O bond hydrolysis. Analysis of

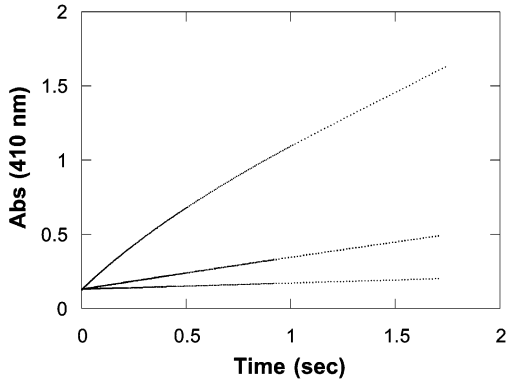

FIGURE 3: Pre-steady-state analysis of PP2Cα mutants R33A and H62Q. Stopped-flow traces of *p*NP formation after rapid mixing in a stopped-flow spectrophotometer of *p*NPP and PP2Cα (top trace), R33A (middle trace), and H62QA (bottom trace) monitored at 410 nm. Reaction conditions consisted of 0.1 M acetate, 0.05 M Tris, 0.05 M Bis-Tris (pH 8.5 @ 25 °C), and 10 mM Mn^{2+}. The final concentration of *p*NPP after mixing was held at 20 mM for wild-type PP2Cα and H62Q, and 150 mM for the R33A mutant. The final concentrations of PP2Cα, R33A and H62QA were 5, 10, and 20 μM, respectively. Reactions were monitored at 410 nm as described under Materials and Methods.

H62Q revealed no initial product burst and was linear across the time range observed (Figure 3), consistent with chemistry being fully rate-limiting, and with H62Q activity impaired at the P−O bond cleavage step.

pH Rate Analysis. In the initial kinetic characterization of PP2Cα (*16*), the pH dependence of k_{cat}/K_m for *p*NPP revealed two ionizations critical for activity, one group that must be unprotonated (pK_a ∼ 7.5) and one group that must be protonated (pK_a ∼ 9). Because of the important nature of His-62 toward catalysis as based by both steady-state (Table 2) and pre-steady-state analysis (Figure 3), we explored whether His-62 might be responsible for one of the ionizations observed in the wild-type PP2Cα pH profile. To test this hypothesis, the pH dependence of k_{cat} and k_{cat}/K_{pNPP} with the H62Q mutant was determined (Figure 4). Mg^{2+} was used as the activating metal due to formation of Mn^{2+} precipitates at high pH (*16*). Except for the order of magnitude decrease in k_{cat} values between wild-type and H62Q enzymes, the shape of the k_{cat} pH profile was similar (Figure 4A), displaying a group that must be unprotonated for activity (pK_a 7.8−8.2). However, analysis of the k_{cat}/K_{pNPP} pH profile revealed a dramatic change (Figure 4B). While an ionization having a pK_a value of 7.7 remained in the H62Q mutant pH profiles, the pK_a of 9.30 observed with wild-type PP2Cα was absent in the H62Q pH profiles of k_{cat}/K_{pNPP}. The loss of the group that must be protonated for activity may be a direct result of the substitution of histidine for glutamine at position 62, suggesting that His-62 is responsible for the higher pK_a and that mutation of this residue eliminates this ionization. These data are consistent with His-62 acting as a general acid during the cleavage of the P−O bond.

Although the H40A mutant displayed no significant adverse effects at pH 8 (Table 2), we determined its activity across a broader pH range and compared the results to those obtained with wild-type and the H62N mutant. The plot of k_{cat} versus pH for the H40A mutant was identical to that of native PP2Cα, revealing an ionization that must be unprotonated and has a pK_a of 7.42 ± 0.09 (data not shown). Also similar to wild-type enzyme, the k_{cat}/K_{pNPP} pH profile for

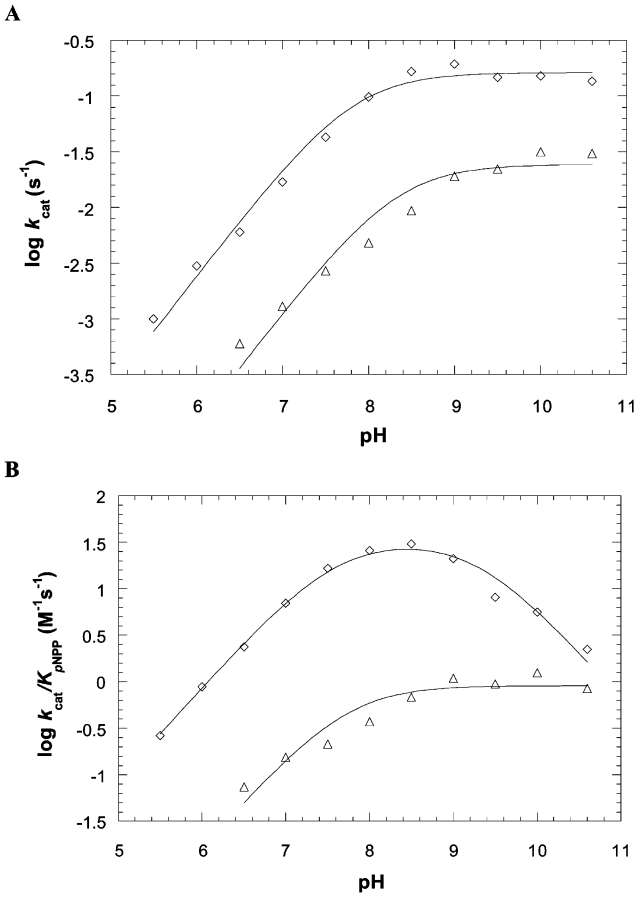

FIGURE 4: Effect of pH on the k_{cat} and k_{cat}/K_{pNPP} parameters at saturating Mg^{2+}. The k_{cat} and k_{cat}/K_{pNPP} values for both wild-type and mutant H62Q were determined by varying the concentration of *p*NPP in saturating Mg^{2+} at the indicated pH values, and fitting the data to the Michaelis−Menten equation. The resulting k_{cat} and k_{cat}/K_{pNPP} values at each pH value were plotted. The pH data for k_{cat} (A) were fitted using the equation $v = C/(1 + H/K_a)$ and yielded pK_a values of 7.82 ± 0.07 and 8.32 ± 0.13 for native enzyme and mutant H62Q, respectively. The wild-type PP2Cα pH data for k_{cat}/K_{pNPP} (B) were fitted using the equation $v = C/(1 + H/K_a + K_b/H)$ and yielded a pK_a value of 7.59 ± 0.10 and pK_b value of 9.30 ± 0.12. The H62Q pH data for k_{cat}/K_{pNPP} (B) were fitted using the equation $v = C/(1 + H/K_a)$ and generated a pK_a value of 7.73 ± 0.13. Open diamonds represent pH data for wild-type PP2Cα and open triangles represent pH data for PP2Cα mutant H62Q. The assay conditions were 0.1 M acetate, 0.05 M Tris, 0.05 M Bis-Tris at 25 °C, 1 mM DTT, and saturating Mg^{2+} (40 mM) and substrate concentrations ranging from 0.1 to 20 mM for wild-type PP2Cα and H62Q or 1−200 mM for R33A. Reactions were assayed using the EDTA endpoint assay as described under Materials and Methods.

H40A revealed two critical ionizations at pK_a 7.37 ± 0.04 and 8.99 ± 0.02 (data not shown). Again, these results are consistent with His-40 playing no significant role in catalysis or substrate binding.

Brönsted Analysis. On the basis of the above pH analysis, we proposed that His-62 could participate in general acid catalysis. To further probe the possibility that His-62 functions as a general acid, a Brönsted analysis was performed using several phosphomonoester substrates with different leaving group pK_a values (Figure 5). For phosphomonoester hydrolysis, Brönsted plots allow the quantification of charge build-up on the leaving group oxygen during the transition state for P−O scission (*16*, *18*−*21*). This analysis is often presented as log k_{cat}/K_m or log k_{cat}

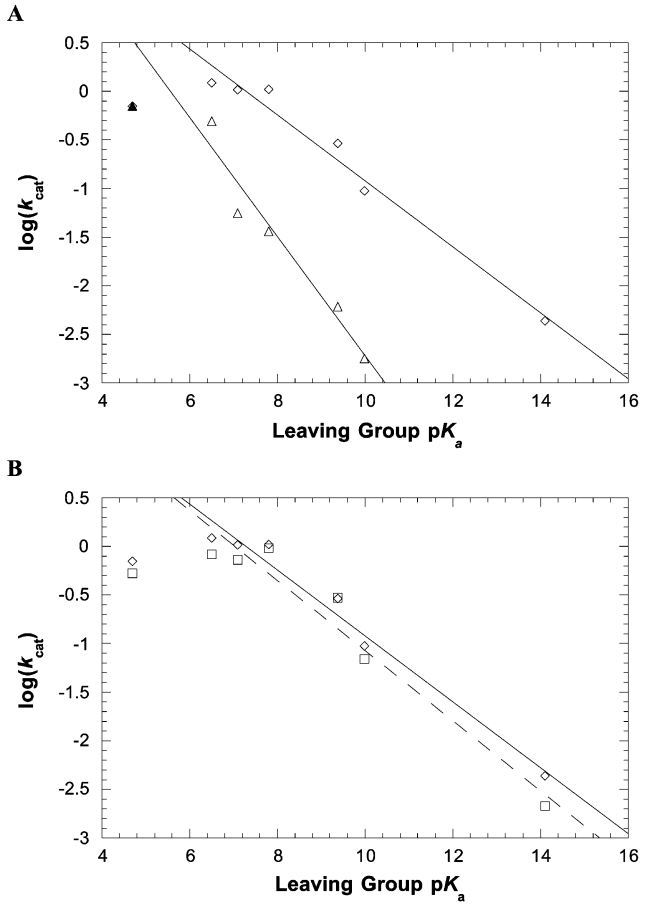

FIGURE 5: Effect of leaving group pK_a value on k_{cat} for PP2Cα mutants H62Q and R33A. Substrates DiFMUP, 6,8-difluoro-4-methylumbelliferyl phosphate (pK_a = 4.6); 8-fluoro-4-methylumbelliferyl phosphate (pK_a = 6.4); *p*NPP (pK_a = 7.1); 4-methylumbelliferyl phosphate (pK_a = 7.8); β-naphthyl phosphate (pK_a = 9.38); phenyl phosphate (pK_a = 9.99); and phosphoserine (pK_a = 14.2) were analyzed under steady-state conditions using the phosphate detection assay at pH 7.0 for wild-type PP2Cα (open diamonds) and PP2Cα mutants H62Q (A) (open triangles) and R33A (B) (open squares). Linear least-squares fitting of the Brönsted plots yielded slopes (β) of −0.33 for wild-type PP2Cα, −0.84 for H62Q, and −0.36 for R33A. The k_{cat} values obtained for DiFMUP and 8-fluoro-4-methyumbelliferyl phosphate were not included for the calculations of β values using wild-type or R33A enzymes (see Results and Discussion). The assay conditions consisted of 0.1 M acetate, 0.05 M Tris, 0.05 M Bis-Tris (pH 7.0 at 25 °C), 1 mM DTT, substrate concentrations ranging from 0.1 to 20 mM for wild-type PP2Cα and H62Q or 1−200 mM for R33A (depending on substrate K_m) and saturating Mn^{2+} (10 mM). Activity was monitored using the phosphate detection assay as described under Materials and Methods.

versus leaving group pK_a. The amplitude of the slope (β-value) from such a plot indicates the extent of charge build-up or proton transfer in the transition state. However, contributions to binding affinity and other steric effects among diverse substrates can be observed from such log k_{cat}/K_m plots. Instead, if the data are presented as log k_{cat} versus pK_a, contributions from steric and binding interactions on the chemical step are minimized. Brönsted analyses have proven useful in examining general-acid catalysis in related phosphatases and other enzymes (*18*−*29*). Although the nature of the rate-limiting step ultimately depends on pH and the pK_a of the leaving group, previous Brönsted analysis with wild-type PP2Cα revealed that the rate-limiting step in catalysis at pH 7.0 was the chemistry step for substrates whose leaving group pK_a values were ∼7 or greater. Under these conditions, a Brönsted slope of −0.32 was obtained (*16*). A similar Brönsted slope of −0.33 was reported for the metal-dependent protein phosphatase calcineurin (*23*), a PPP family member.

To determine whether His-62 donates a proton to the leaving group oxygen, Brönsted analysis was performed with the H62Q mutant at pH 7 (Figure 5). For comparison R33A was analyzed alongside the H62Q mutant. On the basis of the above steady-state analysis, the R33A mutant was predicted to behave similarly to wild-type enzyme. Substrates employed for the Brönsted analysis contained both structurally similar, and structurally distinct compounds (Figure 5). The majority of these substrates were used previously to construct a Brönsted plot of wild-type PP2Cα (*16*). The k_{cat} values for each substrate were determined and plotted against the pK_a value of the leaving group, yielding slopes of −0.84 and −0.36 for mutants H62Q (Figure 5A) and R33A (Figure 5B), respectively. The Brönsted value of −0.36 with the R33A mutant is, within error, identical to that obtained with wild-type enzyme (−0.32). Because the slope of the H62Q mutant was significantly steeper than that of wild-type or R33A enzyme, the magnitude of the slope suggested a greater formation of charge in the transition state than with native PP2Cα or R33A mutant.

With wild-type enzyme, the k_{cat} values obtained with the substrates DiFMUP (pK_a 4.6) and 8-fluoro-4-methyumbelliferyl phosphate (pK_a 6.4) are very similar and do not fall on the Brönsted plot (Figure 5). This break in a Brönsted plot is not uncommon and often reflects a change in the rate-liming step during catalysis. For wild-type PP2Cα, this break was noted previously, and suggested a switch in the rate-limiting step from chemistry to product release (*16*). A similar break was observed when using 2,3,4,5-tetrafluorotyrosine as a substrate for the PPP enzyme calcineurin (*23*). With these excellent leaving groups, chemistry no longer limits the turnover rate, allowing the product release step to become rate-determining at pH 7. For substrates with physiological leaving group pK_a values (≥10), the H62Q mutant is at least 3 orders of magnitude less efficient than wild-type PP2Cα (Figure 5A). However, the catalytic advantage of the wild-type enzyme dissolves as the leaving group pK_a value drops below 6−7, where the H62Q Brönsted plot displays a similar break, albeit at a slightly lower pK_a value. The rates of dephosphorylation of DiFMUP (pK_a 4.6) by H62Q were almost identical to those values obtained with wild-type PP2Cα, indicating that substitution of His-62 for glutamine has no detrimental effect on the value of k_{cat} when the leaving group pK_a is sufficiently low. In contrast, at higher leaving group pK_a values, the difference becomes dramatic. Moreover, these data suggest that the same common phosphate release step limits turnover under these conditions with both wild-type and H62Q enzymes, that His-62 does not function during phosphate release and, more importantly, that His-62 participates during general acid catalysis.

Summary and Concluding Remarks. We determined biochemically that His-62, Arg-33, Asp-60, Asp-239, and Asp-282 are critical catalytic residues within the active site of PP2Cα, the archetypal PPM family member. Although conserved, Thr-128 and His-40 do not function as important residues in catalysis or in metal/*p*NPP binding. However, it

is possible that these residues could function in binding physiological phospho-protein substrates, and thus have been maintained throughout the evolution of many PP2C-like enzymes. We also provide evidence that Arg-33 assists in phosphate binding. Arginine side-chains are often found in the active sites of phosphatases, where similar functions in substrate binding are observed (*30*). In the crystal structure of PP2Cα, Das et al. (*14*) observed two oxygen atoms of inorganic phosphate interacting with the guanidinium group of Arg-33, consistent with the biochemical evidence provided by the R33A mutant.

It was proposed that the ionizable group having a pK_a value of ~7.5 is the water molecule that bridges the two metal atoms in the active site (*16*). There are examples where metal-bound water molecules have been proposed as the nucleophile in which the water molecule has a pK_a value of approximately 7 (*31*, *32*). The PPP family of serine/threonine specific protein phosphatases such as PP1, PP2A, λ phosphatase, and PP2B (calcineurin) also contain dinuclear metal centers, which exhibit a metal-bridged water molecule (*30*). Through the use of crystal structures of protein acid phosphatase (PAP) and PP2B with phosphate or tungstate (*33*−*35*) as well as model studies using simple dinuclear Co(III) complexes (*36*−*39*), strong evidence exists that the bridging water molecule in these systems is the nucleophile used in the dephosphorylation of substrates.

In our efforts to determine the source of the group that must be protonated for catalysis, we evaluated His-40 or His-62 as candidates. The H40A mutant displayed no significant alteration in enzymatic activity, whereas the H62Q mutant displayed impaired catalysis without any detrimental effects on K_m values or phosphate binding. Moreover, the H62Q mutant displayed a loss of the group that must be protonated in the k_{cat}/K_m pH profile, suggesting that His-62 is the important residue that requires protonation. Thus, His-62 may function as the general acid, protonating the leaving group oxygen. Consistent with this, the H62Q mutant displayed a much greater dependence on leaving group pK_a value than the wild-type enzyme (Figure 5A). A large dependence on leaving group pK_a of general acid mutants has been observed for the PTPs, and has been diagnostic in identifying the general acid residue (*18*−*21*). While good leaving groups (low pK_a values) do not necessarily require protonation during P−O cleavage, the protonation of poor leaving groups (high pK_a) becomes more critical for efficient monoester hydrolysis. For example, with *p*NPP as substrate (*p*NP, pK_a = 7.1), the wild-type enzyme is ~30-fold more efficient than the H62Q enzyme (Figure 5). With a physiological substrate like phospho-serine (serine pK_a = 14.2), the wild-type enzyme would be 1000-fold more efficient than the H62Q mutant. With DiFMUP (DiMU pK_a = 4.6), almost no difference in k_{cat} values between wild-type and the H62Q mutant were observed (Figure 5).

Das et al. did not propose a role for His-62, due to the observation that His-62 was flipped away from the dinuclear metal center in the crystal structure (*14*). The distance between the phosphate oxygens and His-62 was greater than 5 Å. It is important to note that the crystals were grown at pH 5, where PP2Cα has only ~0.1% of its optimal activity found at pH 8. Also, this structure is an inhibited complex with inorganic phosphate bound, not an authentic Michaelis-Complex. Using molecular modeling, the side-chain of His-62 can easily rotate closer to the active site, where the side-chain would be only 2.4 Å from the phosphate and therefore in position to participate in catalysis. His-62 resides on the bottom of the catalytic cleft and when rotated toward the active site, does not introduce any steric clashes with other residues in close proximity to the metal center. Collectively, our results suggest that His-62 is the active site residue that must be protonated for activity, and participates during proton donation to the leaving group oxygen, perhaps acting directly as the general acid.

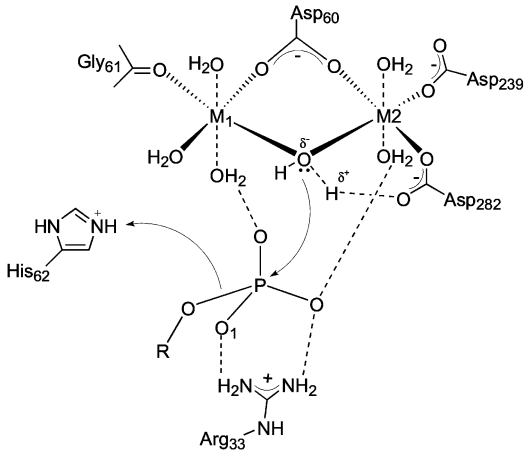

FIGURE 6: Proposed mechanism for protein dephosphorylation catalyzed by PP2Cα. Asp-282 may play a role in activating the metal-associated water molecule for nucleophilic attack at the phosphorus atom in a S_N2 mechanism. The substrate is positioned close to the metal center by hydrogen-bonds to metal-bound water molecules and by electrostatic interactions with Arg-33, which also functions during transition-state stabilization. To facilitate leaving group expulsion from physiological substrates, the conserved His-62 residue may protonate the leaving group oxygen atom, acting as a general acid during catalysis.

From this work, we propose a mechanism for phosphate hydrolysis catalyzed by PP2Cα. As shown in Figure 6, hydrolysis of the phosphorylated substrate is facilitated by the activation of the water molecule coordinated to the two metal centers and hydrogen-bonded to Asp-282. These two events would make the water molecule more nucleophilic in the hydrolysis of substrate. The nucleophilic water molecule thus reacts with the phosphate, which is partly held in place by the guanidinium side-chain interactions of Arg-33. During P−O bond cleavage, the leaving group is protonated either directly or indirectly by His-62, acting as a putative general acid.

ACKNOWLEDGMENT

The authors wish to thank Dr. Kirk Tanner and Mr. Michael Langer for helpful discussions, and Drs. Alvan Hengge (Utah State University) and Ron Raines (University of Wisconsin) for discussions on Brönsted analyses. We would also like to thank Dr. Kyle Gee (Molecular Probes) for generous samples of 8-fluoro-4-methylumbelliferyl phosphate.

REFERENCES

1. Denu, J. M., Stuckey, J. A., Saper, M. A., and Dixon, J. E. (1996) *Cell 87*, 361−4.
2. Barford, D. (1996) *Trends Biochem. Sci. 21*, 407−12.
3. Fauman, E. B., Yuvaniyama, C., Schubert, H. L., Stuckey, J. A., and Saper, M. A. (1996) *J. Biol. Chem. 271*, 18780−8.

4. Barford, D., Das, A. K., and Egloff, M. P. (1998) *Annu. Rev. Biophys. Biomol. Struct. 27*, 133−64.
5. Rusnak, F. (2000) *Met. Ions Biol. Syst. 37*, 305−43.
6. Cohen, P., and Cohen, P. T. (1989) *J. Biol. Chem. 264*, 21435−8.
7. Cohen, P. (1989) *Annu. Rev. Biochem. 58*, 453−508.
8. Takekawa, M., Maeda, T., and Saito, H. (1998) *EMBO J. 17*, 4744−52.
9. Hanada, M., Kobayashi, T., Ohnishi, M., Ikeda, S., Wang, H., Katsura, K., Yanagawa, Y., Hiraga, A., Kanamaru, R., and Tamura, S. (1998) *FEBS Lett. 437*, 172−6.
10. Strovel, E. T., Wu, D., and Sussman, D. J. (2000) *J. Biol. Chem. 275*, 2399−403.
11. Leung-Hagesteijn, C., Mahendra, A., Naruszewicz, I., and Hannigan, G. E. (2001) *EMBO J. 20*, 2160−70.
12. Travis, S. M., Berger, H. A., and Welsh, M. J. (1997) *Proc. Natl. Acad. Sci. U.S.A. 94*, 11055−60.
13. Zhu, T., Dahan, D., Evagelidis, A., Zheng, S., Luo, J., and Hanrahan, J. W. (1999) *J. Biol. Chem. 274*, 29102−7.
14. Das, A. K., Helps, N. R., Cohen, P. T., and Barford, D. (1996) *EMBO J. 15*, 6798−809.
15. Zhou, G., Denu, J. M., Wu, L., and Dixon, J. E. (1994) *J. Biol. Chem. 269*, 28084−90.
16. Fjeld, C. C., and Denu, J. M. (1999) *J. Biol. Chem. 274*, 20336−43.
17. Brotherus, J. R., Jacobsen, L., and Jorgensen, P. L. (1983) *Biochim. Biophys. Acta 731*, 290−303.
18. Rigas, J. D., Hoff, R. H., Rice, A. E., Hengge, A. C., and Denu, J. M. (2001) *Biochemistry 40*, 4398−406.
19. Fjeld, C. C., Rice, A. E., Kim, Y., Gee, K. R., and Denu, J. M. (2000) *J. Biol. Chem. 275*, 6749−57.
20. Zhang, Y. L., Hollfelder, F., Gordon, S. J., Chen, L., Keng, Y. F., Wu, L., Herschlag, D., and Zhang, Z. Y. (1999) *Biochemistry 38*, 12111−23.
21. Zhao, Y., and Zhang, Z. Y. (1996) *Biochemistry 35*, 11797−804.
22. Han, R., and Coleman, J. E. (1995) *Biochemistry 34*, 4238−45.
23. Martin, B. L., and Graves, D. J. (1993) *Biochem. Biophys. Res. Commun. 194*, 150−6.
24. Martin, B., Pallen, C. J., Wang, J. H., and Graves, D. J. (1985) *J. Biol. Chem. 260*, 14932−7.
25. McCain, D. F., Catrina, I. E., Hengge, A. C., and Zhang, Z. Y. (2002) *J. Biol. Chem. 277*, 11190−200.
26. MacLeod, A. M., Tull, D., Rupitz, K., Warren, R. A. J., and Withers, S. G. (1996) *Biochemistry 35*, 13165−13172.
27. Thompson, J. E., and Raines, R. T. (1994) *J. Am. Chem. Soc. 116*, 5467−5468.
28. Zhang, Z.-Y., Wang, Y., and Dixon, J. E. (1994) *Proc. Natl. Acad. Sci. U.S.A. 91*, 1624−1627.
29. Toney, M. D., and Kirsch, J. F. (1989) *Science 243*, 1485−1488.
30. Jackson, M. D., and Denu, J. M. (2001) *Chem. Rev. 101*, 2313−40.
31. Chen, G., Edwards, T., D'souza, V. M., and Holz, R. C. (1997) *Biochemistry 36*, 4278−86.
32. Pohjanjoki, P., Lahti, R., Goldman, A., and Cooperman, B. S. (1998) *Biochemistry 37*, 1754−61.
33. Goldberg, J., Huang, H. B., Kwon, Y. G., Greengard, P., Nairn, A. C., and Kuriyan, J. (1995) *Nature 376*, 745−53.
34. Egloff, M. P., Cohen, P. T., Reinemer, P., and Barford, D. (1995) *J. Mol. Biol. 254*, 942−59.
35. Klabunde, T., Strater, N., Frohlich, R., Witzel, H., and Krebs, B. (1996) *J. Mol. Biol. 259*, 737−48.
36. Wahnon, D., Lebuis, A.-M., and Chin, J. (1995) *Angew. Chem. Int. Ed. Engl. 34*, 2412−2414.
37. Williams, N. H., and Chin, J. (1996) *J. Chem. Soc, Chem. Commun*. 131−132.
38. Williams, N. H., Cheung, W., and Chin, J. (1998) *J. Am. Chem. Soc. 120*, 8079−8087.
39. Humphry, T., Forconi, M., Williams, N. H., and Henge, A. C. (2002) *J. Am. Chem. Soc. 124*, 14860−14861.

BI034074+